

**DIAGNOSTYKA**, 2025, Vol. 26, No. 4

**e-ISSN** 2449-5220 **DOI:** 10.29354/diag/213789

# DESIGN OF MOTOR BEARING FAULT DIAGNOSIS METHOD BASED ON IMPROVED GWO-SVM

Lijuan CHANG 💿

School of Intelligent Manufacturing, Hebi Polytechnic, Hebi, 458030, China Corresponding author, e-mail: <a href="mailto:changlijuan100@163.com">changlijuan100@163.com</a>

#### Abstract

Electric motors are the core equipment of industrial production, and rolling bearings are the key parts that are most prone to failure during the operation of electric motors. In order to accurately diagnose bearing faults and improve equipment reliability, this study extracts features from motor vibration signals through ensemble empirical mode decomposition, and classifies signal features using support vector machines. In addition, an optimized GWO is introduced to improve the hyperparameter settings of the support vector machine model, enhancing the fault classification ability, and ultimately constructing a new diagnosis model. The new model had the highest fault classification accuracy of 96.6%, the highest precision of 94.58%, the highest F1 score of 95.18%, and the shortest running time of 8.07 seconds. In addition, its MSE, RMSE, and MAE for outer ring fault detection were the lowest, at 0.072, 0.268, and 0.189, respectively, with a diagnosis time of 7.33 seconds, significantly better than comparison models. From this, the model can enhance the diagnosis accuracy and efficiency, and also provide an effective solution for motor bearing fault diagnosis in industrial applications.

Keywords: Electric motor bearings; Fault diagnosis; SVM; GWO; EEMD

#### 1. INTRODUCTION

The bearing components in an electric motor can directly affect the rotational efficiency and service life of the motor. However, during long-term and high load operation, bearings are prone to malfunctions such as raceway wear, pitting corrosion, and fracture due to factors such as friction, wear, poor lubrication, and external environment [1-2]. These issues reduce the efficiency of the electric motor, but may also lead to system shutdown or even serious safety accidents. Therefore, researchers at home and abroad have successively explored methods for diagnosing motor bearing faults. Dong et al. believed that existing Bearing Fault Diagnosis (BFD) methods were based on processing data from a single source and did not have universality. Therefore, a method on the basis of multi-source data and 1D lightweight Convolutional Neural Network (CNN) was proposed. This method had stronger accuracy and robustness compared to other advanced methods [3]. Zhukovskiy et al. built a novel diagnostic method for electric motor faults on the basis of parameter analysis, which combined singular value decomposition and hierarchical clustering to improve the efficiency. The motor fault diagnosis time and accuracy were significantly improved compared to before the improvement [4].

Xu et al. found that due to parameter settings and adjustments, the effectiveness and accuracy of Petri networks for BFD were poor. Therefore, a comprehensive fuzzy Petri network was designed for motor BFD. The network achieved better performance in fault localization [5]. Wang et al. found that the noise interference and signal measurement errors of motor bearings to some extent interfered with the accuracy of later data processing. Therefore, an industrial motor BFD model was proposed. This method solved the height conflicts in the data fusion process and improved the diagnostic accuracy [6].

Artificial intelligence technology has provided new research ideas for BFD. Among them, Support Vector Machine (SVM), as a classic machine learning method, has high classification accuracy and generalization ability under small sample conditions, and has been largely used in fault diagnosis [7]. Brusamarello et al. found that there were still certain deficiencies in the detection of motor shaft faults based on fiber Bragg grating analysis. To this end, a fault grating signal classification and recognition model that combined SVM was proposed. The signal classification accuracy was 92.73%, indicating high effectiveness [8]. Zhou et al. built a rolling BFD model on the basis of the Whale Grey Wolf Optimization (GWO)-

Received 2025-01-15; Accepted 2025-10-31; Available online 2025-11-06

<sup>© 2025</sup> by the Authors. Licensee Polish Society of Technical Diagnostics (Warsaw. Poland). This article is an open access article distributed under the terms and conditions of the Creative Commons Attribution (CC BY) license (<a href="http://creativecommons.org/licenses/by/4.0/">http://creativecommons.org/licenses/by/4.0/</a>).

Variational Mode Decomposition-SVM (VMD-SVM) to deal with unclear fault characteristics. The highest accuracy of this method after multiple repeated tests was 95.73%, which was superior to other existing methods [9]. Yang et al. built a coupled vibration data classification strategy on the basis of triple embedding and SVM to classify small sample datasets. Compared with traditional features and autoencoders, this method had better data classification performance and stronger stability [10]. Wang et al. fused CNN and SVM to achieve rolling BFD. Compared with other methods, this algorithm significantly improved the accuracy, with an accuracy rate of up to 93.01% [11].

In summary, significant progress has been made in improving the accuracy and efficiency of BFD through existing research. However, these methods still have problems such as strong dependence on specific scenarios, insufficient ability to adapt to complex non-stationary signals, and limited efficiency in parameter optimization. To this end, a novel BFD model for motor rolling bearings on the basis of improved GWO and SVM is built. This method improves the hyperparameter optimization efficiency of SVM models by introducing dynamic adaptive guidance factors and backup location strategies to optimize the global search and local development capabilities of GWO. The innovation lies in the proposed improved algorithm, which effectively avoids the model falling into local optima, and optimizes the ability to classify complex nonlinear signal features. At the same time, its strong adaptability and promotability make it widely applicable in multiple fields such as electricity, manufacturing, and transportation, effectively improving the reliability and safety of equipment operation and promoting the transformation of traditional industries towards intelligence and digitization. Provided key technical support for building safe and efficient industrial systems, and contributed to energy conservation, emission reduction, resource optimization, and sustainable social development.

#### 2. METHODS AND MATERIALS

### 2.1. Feature extraction of vibration signals of motor rolling bearings based on SVM

To improve the accuracy and efficiency of fault diagnosis of motor rolling bearings, a new type of motor rolling bearing fault diagnosis model is proposed by combining improved GWO and SVM. The process is shown in Figure 1.

In Figure 1, the new model mainly involves five key steps. Firstly, the vibration signals of the motor rolling bearings are obtained through a fault simulation platform and subjected to data preprocessing such as standardization and denoising to ensure the quality and consistency of the signals. Secondly, EEMD decomposes the pre-processed signal and extracts key feature vectors in both timeand frequency-domain. Then, SVM classifier classifies different types of fault signals. In this process, the improved GWO is introduced to optimize SVM hyperparameters. Specifically, the improved GWO enhances the global search capability and local development efficiency through dynamic adaptive guidance factors and backup position strategies, effectively avoiding falling into local optima. Finally, the diagnosis performance of the method is validated through model training and testing. As a key component of an electric motor, rolling bearings support the rotor through rolling elements and reduce friction. They are mainly composed of an inner ring, an outer ring, rolling elements, and a cage, which are used to bear the radial and axial loads of the motor, ensuring the stable rotation and efficient operation of the rotor [12-13]. Rolling bearings can replace sliding contact with rolling contact, significantly reduce friction coefficient, improve transmission efficiency, and have compact structure, strong durability, and smooth operation. According to the different rolling elements, rolling bearings can be divided into various types such as deep groove ball bearings, cylindrical roller bearings, and angular contact ball bearings to meet various working conditions. The

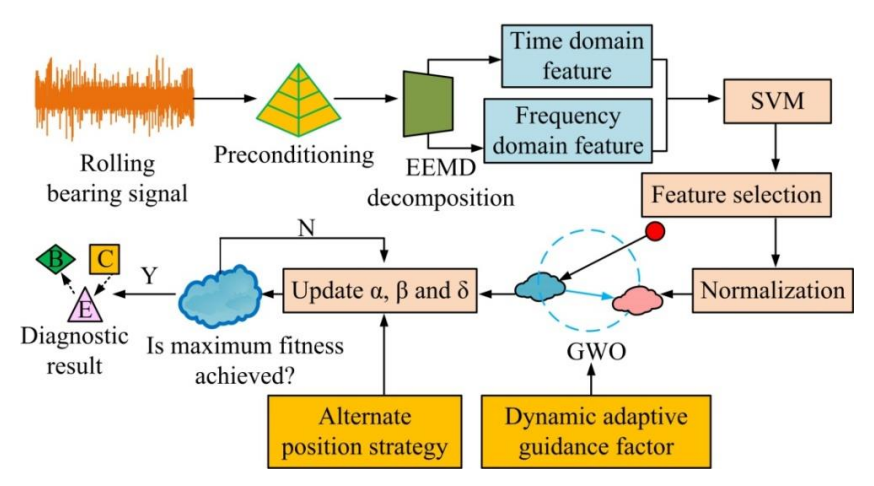


Fig. 1. New motor rolling bearing fault diagnosis model flow

physical and structural diagrams of the motor rolling bearing are displayed in Figure 2 [14].



(a) Motor rolling bearing physical drawing

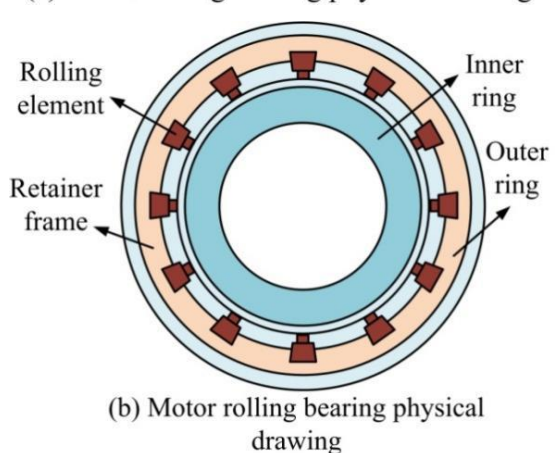


Fig. 2. Motor rolling bearing physical drawing and structure drawing

Figure 2 (a) shows the physical image of the motor rolling bearing, and Figure 2 (b) displays the motor rolling bearing. In Figure 2, the motor rolling bearing has an outer ring, an inner ring, a retainer frame, and a rolling element. Among them, the outer ring is fastened on the equipment casing, and the inner ring is linked to the rotating shaft. The outer and inner rings respectively serve to fix and support the bearing, and the rolling elements perform rolling motion between these two rings through the retainer frame, thereby achieving a low friction rotational effect. In addition, vibration signals are an important representation of the operating status, which reflects the dynamic characteristics of bearings under normal operation or fault conditions [15-16]. The research adopts the motor fault simulation platform developed by Zongyuan Measurement Company for fault data collection [17]. The motor speed is 1786rpm and the sampling frequency is 12 kHz. Time-domain diagrams of bearing signals are plotted. The time-domain diagrams of bearings under various conditions are displayed in Figure 3.

Figure 3 (a) displays the bearing signal in four faults. According to Figure 3, under normal operating conditions, the vibration signal fluctuates relatively smoothly without obvious impact characteristics. Under the inner ring, outer ring, and

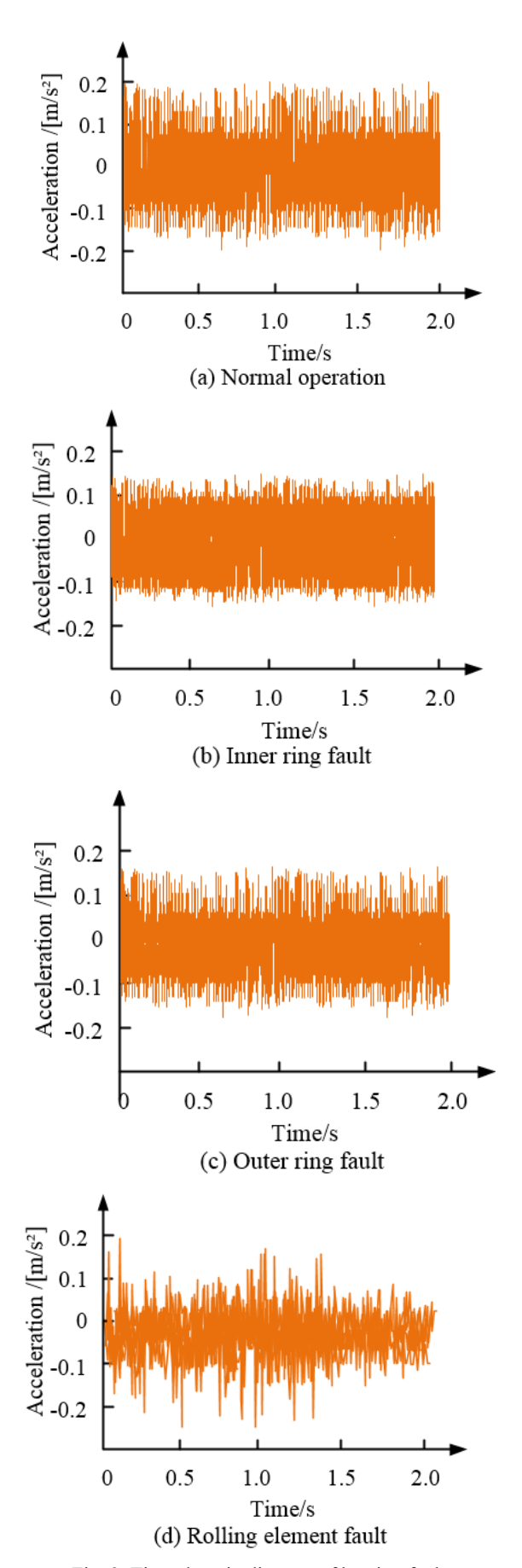


Fig. 3. Time-domain diagram of bearing fault under various working conditions

rolling elements, varying degrees of periodic impact are observed in the vibration signal, with significantly increased amplitude and fluctuation. Among them, the signal complexity of rolling element faults is the highest, and feature information is difficult to extract directly. The experimental platform used for simulating faults in rolling bearings of electric motors is shown in Figure 4.



Motor DAQ Accelerometer Monitor Fig. 4. Experimental test platform and sensor layout

In Figure 4, the motor is connected to the bearing seat through a shaft, and an acceleration sensor is installed on the bearing housing to collect vibration signals. The Data Acquisition (DAQ) module inputs signals into the data processing computer. All key components have been marked with arrows. To further separate and extract fault features from bearing vibration signals, the Ensemble Empirical Mode Decomposition (EEMD) method is introduced in the study. Compared to other methods, EEMD has significant advantages, including the ability to handle non-stationary signals and effectively reduce pattern aliasing problems. The basic idea is to decompose complex signals into several Intrinsic Mode Functions (IMFs) by introducing white noise perturbations, achieving component extraction of the original signal [18]. Firstly, multiple sets of independent white noise are applied to the original vibration signal to construct multiple sets of superimposed signals. The calculation is displayed in equation (1).

$$x_i(t) = x(t) + w_i(t) \tag{1}$$

In equation (1), x(t) signifies the original signal.  $w_i(t)$  represents independent white noise.  $x_i(t)$  represents the signal after the i-th addition of noise. Each group of signals undergoes EEMD decomposition to obtain several IMFs components, as displayed in equation (2).

$$x_{i}(t) = \sum_{j=1}^{n} IMF_{ij}(t) + r_{i}(t)$$
 (2)

In equation (2),  $IMF_{ij}(t)$  represents the j-th IMF component obtained from the i-th decomposition.  $r_i(t)$  represents the remaining residuals. After completing the EEMD decomposition, to achieve accurate identification and classification of bearing fault characteristics, SVM is further introduced as a fault classification model. SVM can effectively distinguish fault features of various categories by constructing the optimal classification hyperplane. The classification principle diagram of SVM is shown in Figure 5.

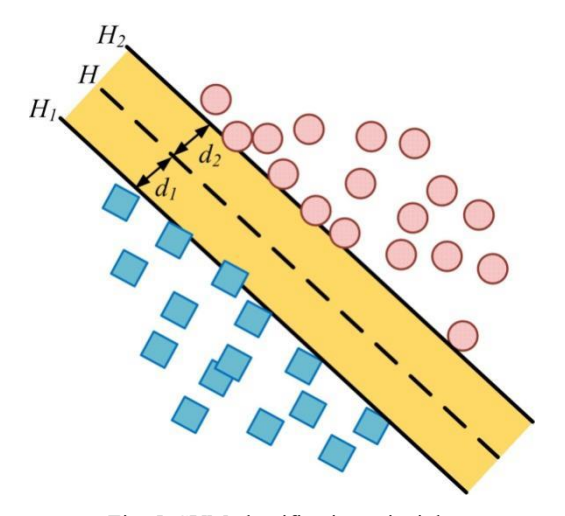


Fig. 5. SVM classification principle schematic diagram

As shown in Figure 5, the red dots and blue squares represent samples of different categories. The dashed line H represents the optimal classification hyperplane, and the solid lines  $H_1$  and  $H_2$  represent the boundaries of the classification interval. The two types of sample points are distributed on both sides of the boundary. The classification interval is defined as the distance between two boundaries  $H_1$  and  $H_2$ , i.e.  $(d_1 + d_2)$ . Among them, the data points closer to the decision boundary are support vectors. To define this decision boundary, it is generally approximated by calculating  $(d_1 + d_2)$ , as shown in equation (3).

$$D = \{(x_i, y_i) | i = 1, 2, \dots, n\}, x_i \in R, y_i \in \{1, -1\}$$
(3)

In equation (3), D signifies a complete dataset.  $x_i$  and  $y_i$  respectively signify two 2D data points on the dataset. The dataset is correctly classified as a straight line, as displayed in equation (4).

$$\begin{cases} wx_1 + b = 1\\ wx_2 + b = -1 \end{cases}$$

$$(4)$$

In equation (4), w and b represent the weights and biases of the samples belonging to the given dataset, respectively.  $x_1$  and  $x_2$  represent the support vectors on the positive and negative class boundaries, respectively. The distance between  $H_1$  and  $H_2$  and the decision boundary is calculated, as shown in equation (5).

$$\begin{cases} d_{1} = \frac{|wx_{1} + b|}{\|w\|} = \frac{1}{\|w\|} \\ d_{2} = \frac{|wx_{2} + b|}{\|w\|} = \frac{1}{\|w\|} \\ d_{1} + d_{2} = \frac{2}{\|w\|} \end{cases}$$
 (5)

After taking the derivative of equation (5), the classification optimization objective of the feature vector is represented by the SVM, as displayed in equation (6).

$$M_{total} = \min \frac{1}{2} ||w||^2 + C \sum_{i=1}^{N} \varsigma_i$$
 (6)

In equation (6),  $\varsigma_i$  signifies the relaxation variable of the i-th data point. C signifies the penalty coefficient.  $M_{total}$  represents the final timedomain signal classification feature of rolling bearings.

### 2.2. Construction of rolling bearing fault diagnosis model integrating improved GWO

After collecting specific motor rolling bearing signal data, the signals are decomposed and reconstructed using the EEMD method, and relevant features are extracted. After combining SVM for data classification and diagnosis, although SVM shows good accuracy in classification tasks, its performance is still affected to some extent by model hyperparameters, such as penalty factors, kernel function parameters, and input feature selection. If the hyperparameter selection is improper, it may lead to a decrease in classification accuracy or insufficient model generalization ability [19]. For this purpose, GWO is introduced to optimize the hyperparameters of SVM models. Compared to traditional grid search or particle swarm optimization algorithms, GWO has higher efficiency convergence in solving multidimensional parameter optimization problems. The gray wolf position update in GWO is shown in Figure 6 [20].

During the hunting process in Figure 6, individuals in the gray wolf population has three levels, namely  $\alpha$ ,  $\beta$ , and  $\delta$ , representing the best, second, and third solutions in the population, respectively, and represented by green, yellow, and blue colors. Among them, the ordinary wolf, also known as the red individual, calculates its new position based on its relative position with these three key individuals, which includes calculating distances  $D_{\alpha}$ ,  $D_{\beta}$ , and  $D_{\delta}$  as well as adjusting its direction. Finally, the search for the optimal solution is completed by approaching the prey through

multiple iterations. The operation process of GWO is shown in Figure 7.

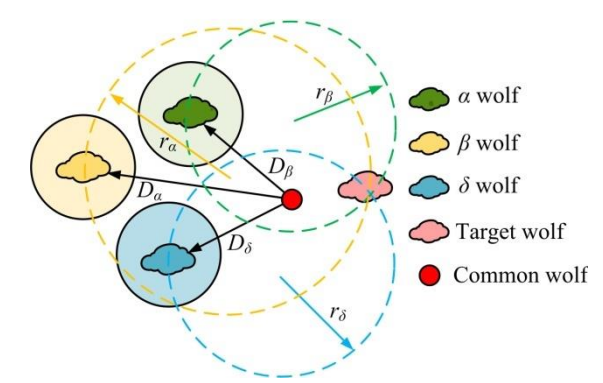


Fig. 6. GWO location update diagram

As shown in Figure 7, firstly, the algorithm randomly initializes the position and related parameters of the grey wolf population, such as control population size and parameters. Subsequently, the current positions of individuals in the grey wolf population are evaluated using fitness functions. The top three individuals with the best fitness are taken as  $\alpha$ ,  $\beta$ , and  $\delta$ , respectively. In each iteration, the position of the regular wolf will be dynamically updated on the basis of the guidance information of the  $\alpha$ ,  $\beta$ , and  $\delta$ . The iterative process performs until predetermined termination conditions are satisfied, like reaching the maximum iteration or convergence of fitness to the optimal value. The expression for updating individual positions is displayed in equation (7).

$$X(k+1) = \frac{1}{3}(X_{\alpha}(k) + X_{\beta}(k) + X_{\delta}(k))$$
 (7)

In equation (7), X(k+1) signifies the position vector of the gray wolf in the k+1-th.  $X_{\alpha}(k)$ ,  $X_{\beta}(k)$  and  $X_{\delta}(k)$  signify the position vectors of  $\alpha$ ,  $\beta$ , and  $\delta$  in the k-th iteration. At this point, after continuous optimization iterations, the final position is updated, as displayed in equation (8).

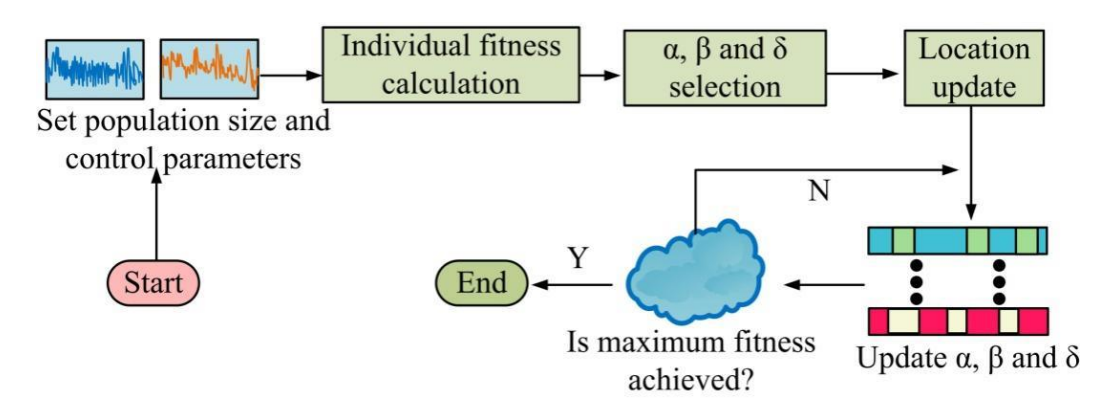


Fig. 7. GWO operation flow

$$\begin{cases} X_i(k+1) = X_p(k) - A \cdot d_G \\ d_G = \left| E \cdot X_p(k) - X_i(k) \right| \end{cases}$$
(8)

In equation (8),  $X_i(k+1)$  signifies the new position of the i-th gray wolf in the k+1-th.  $X_{p}(k)$  signifies the position of the leader wolf  $\alpha$ ,  $\beta$ , or  $\delta$  in the k-th. A and E both signify constants. a represents a linearly decreasing regulatory factor.  $d_{\rm G}$  signifies the distance between the grey wolf and its prey. However, as the highest ranking level in the pack of wolves, a wolves rely too much on the current optimal solution and have local optima, especially in high-dimensional and non-convex problems, which may lead to a decrease in global search ability and affect the overall optimization effect. To this end, a backup location strategy is designed for a wolves. A random perturbation mechanism is introduced to generate new exploration points near the current location of  $\alpha$ wolves, improving the search ability of the population. The calculation for generating backup positions is displayed in equation (9).

$$X_{\alpha}^{new} = X_{\alpha} + \mu \cdot (X_{\beta} - X_{\delta}) + \lambda \cdot rand(-1,1) \quad (9)$$

In equation (9),  $X_{\alpha}^{\text{new}}$  and  $X_{\alpha}$  signify the backup position and current iteration position of  $\alpha$  wolf, respectively.  $X_{\beta}$  and  $X_{\delta}$  respectively signify the positions of  $\beta$  wolf and  $\delta$  wolf in the current iteration.  $\mu$  represents the regulatory factor that controls the balance between global and local search.  $\lambda$  represents the disturbance intensity factor. The distance correction is shown in equation (10).

$$d_{\alpha}^{new} = \left\| X_{\alpha}^{new} - X_{prey}^{1} \right\| \tag{10}$$

In equation (10),  $d_{\alpha}^{new}$  signifies the distance between the backup position and the prey.  $X_{prey}$  signifies the prey position. In addition, the study introduces dynamic adaptive guidance factors to flexibly adjust the impact weights of the three factors on population search according to different iteration stages. Specifically, increasing the weight of  $\alpha$  wolf in the early stages realizes global exploration, while increasing the weight of  $\beta$  wolf and  $\delta$  wolf in the later stages enables local development. The calculation for dynamically guiding factor weight is shown in equation (11).

$$\begin{cases} \mathcal{G}_{\alpha}(k) = 1 - \frac{k}{K_{\text{max}}} \\ \mathcal{G}_{\beta}(k) = 1 - \frac{k}{K_{\text{max}}} \\ \mathcal{G}_{\delta}(k) = 1 - \frac{k}{K_{\text{max}}} \cdot \eta \end{cases}$$
(11)

In equation (11),  $\mathcal{G}_{\alpha}(k)$ ,  $\mathcal{G}_{\beta}(k)$ , and  $\mathcal{G}_{\delta}(k)$  respectively represent the guiding factors of  $\alpha$ ,  $\beta$ , and  $\delta$  at the k-th iteration.  $\eta$  represents the adjustment

parameter used to control the guiding proportion of  $\beta$  wolf and  $\delta$  wolf.  $K_{\text{max}}$  represents the maximum number of iterations. At this point, the improved position update is shown in equation (12).

$$X_{i}(k+1) = \mathcal{G}_{\alpha}(k) \cdot X_{\alpha} + \mathcal{G}_{\beta}(k) \cdot X_{\beta}(k) + \mathcal{G}_{\delta}(k) \cdot X_{\delta}(k)$$
(12)

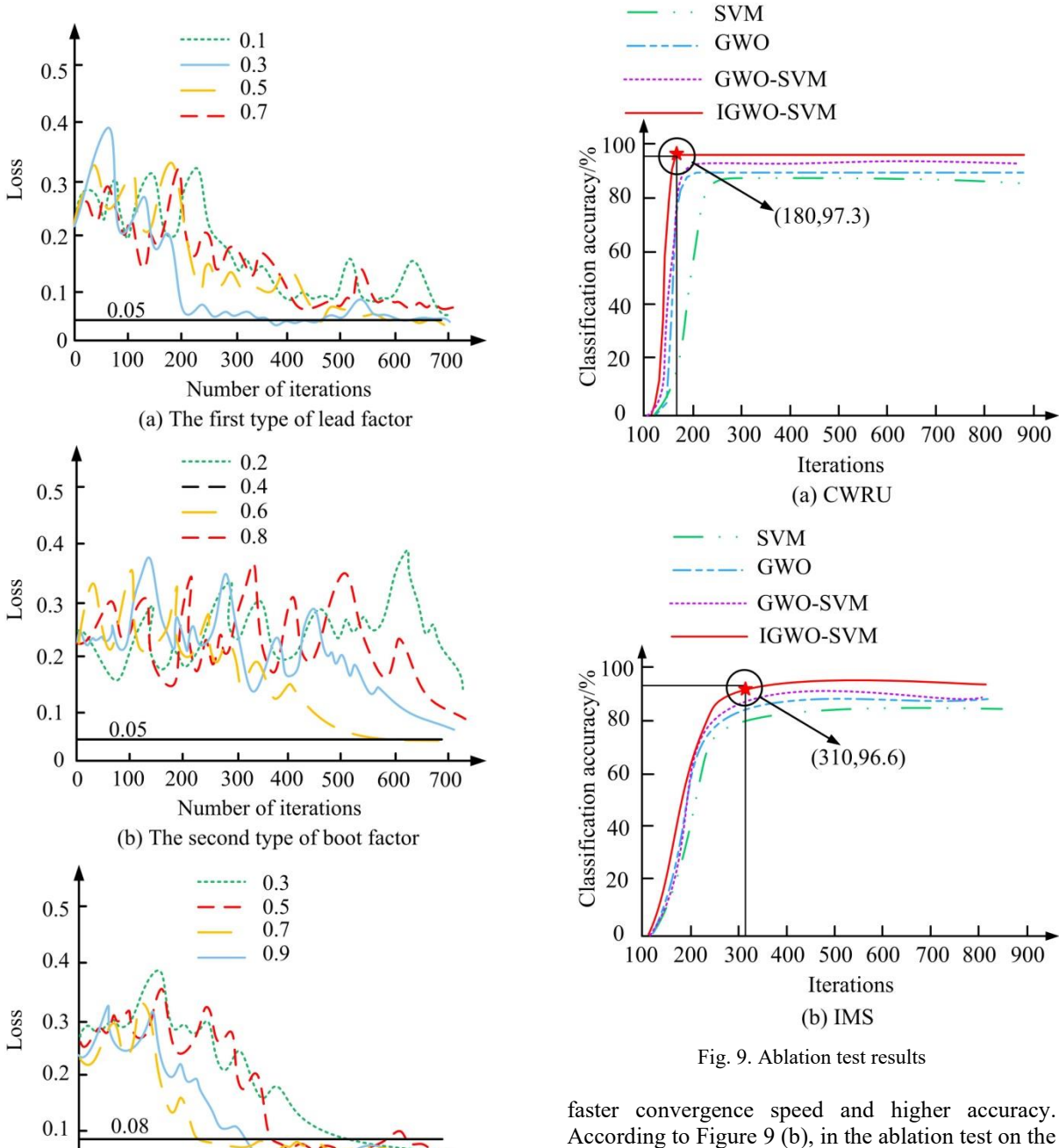
According to equation (12), the position of gray wolf individual  $X_i$  in the k+1st generation can be obtained.

#### 3. RESULTS

### 3.1. Performance testing of the new fault diagnosis model for motor rolling bearings

To validate the new motor rolling BFD model, the CPU is set to Intel Core i7-10700K, the base frequency is 3.8 GHz, the GPU is NVIDIA GeForce RTX 3080, the video memory is 10 GB, the memory is 32 GB, and the operating system is Windows 10. The Case Western Reserve University Bearing Data Center Dataset (CWRU) and the Intelligent Maintenance Systems Bearing Dataset (IMS) are taken as the testing data sources. The CWRU is simulated using an electric motor fault simulator, collecting vibration signal data including normal state, inner ring fault, outer ring fault, and rolling element fault. The IMS dataset is collected throughout the entire life cycle of bearings, containing vibration signals of multiple bearings from normal state to failure. The data collection environment is close to the real industrial environment. The study first conducts hyperparameter selection tests on the three guiding factors of  $\alpha$ ,  $\beta$ , and  $\delta$ , namely  $\mathcal{G}_{\alpha}(t)$ ,  $\mathcal{G}_{\beta}(t)$ , and  $\mathcal{G}_{s}(t)$ . The test results are shown in Figure 8.

Figure 8 shows the test results of  $\mathcal{G}_{\alpha}(t)$ ,  $\mathcal{G}_{\beta}(t)$ , and  $\theta_{s}(t)$ . As shown in Figure 8, when the  $\theta_{\alpha}(t)$  is 0.5, the convergence speed was the fastest, and the final loss value stabilized at around 0.05. In other values, the convergence speed was significantly slower, especially when the value was 0.1, the Loss value remained above 0.15 after 700 iterations. For  $\mathcal{G}_{g}(t)$ , when the value was 0.4, the final loss value of the model dropped to around 0.08, demonstrating optimal convergence. When the value was 0.8, the convergence was unstable and the final loss value remained around 0.2. For  $\mathcal{G}_{s}(t)$ , at 0.7, the model exhibited the best convergence speed and stability, with a final loss value of approximately 0.07. Other values may lead to premature convergence, resulting in a final loss value of around 0.12. Based on the above analysis, the optimal values of the guidance factors for  $\alpha$ ,  $\beta$ , and  $\delta$  are selected as 0.5, 0.4, and 0.7. respectively, to ensure the convergence speed and optimal performance. The study continues to conduct ablation tests on the final IGWS-SVM model, as presented in Figure 9.



0

100

200

300 400

Number of iterations

(c) The third class of regulatory factors

Fig. 8. Hyperparameter selection test result

dataset, and Figure 9 (b) displays the results in the

IMS dataset. In Figure 9 (a), the classification

accuracy of using SVM alone tended to stabilize

after 200 iterations, ultimately reaching about

80.1%. The GWO-SVM model combined with

GWO has improved classification performance

compared to the SVM model, with an accuracy rate

of approximately 90.2% after 300 iterations. The

improved IGWS-SVM model further improved the

classification performance, with a classification

accuracy of 97.3% in 180 iterations, demonstrating

Figure 9 (a) displays the results in the CWRU

500

600

700

According to Figure 9 (b), in the ablation test on the IMS dataset, although there was a significant improvement in the classification accuracy in SVM alone and the GWO-SVM model, there were still shortcomings compared to the final IGWS-SVM model. Especially in 310 iterations, IGWS-SVM achieved a classification accuracy of 96.6%. This indicates that improving GWO and combining it can significantly enhance SVM effectiveness of signal detection and classification. The study introduces other advanced methods, such as Deep Residual CNN (DR-CNN), Multiscale CNN (MSCNN), and VMD-SVM, as presented in Table 1, taking precision, recall, F1 score, and running time as indicators for classification.

According to Table 1, in the CWRU dataset, the improved model achieved a classification precision of 95.73%, a recall rate of 94.58%, an F1 score of 95.18%, and a running time of only 8.33 seconds. Compared with VMD-SVM, it improved

classification performance by 5.52%, 2.44%, and 2.15%, respectively, and shortened running time by about 2.12 seconds. In the IMS dataset, the improved model had classification precision, recall, and F1 of 95.02%, 93.22%, and 94.14%. Compared to the second best performing VMD-SVM, it improved by 3.45%, 1.94%, and 2.77%, respectively, and reduced running time to 8.07 seconds. This indicates that the proposed method not only achieves significant improvement in classification performance indicators, but also demonstrates high computational efficiency, verifying its superiority and practical application value.

Table 1. Multiple indicator test results

Data set	Algorit hm	Precisio n/%	Recall /%	F1/ %	Runni ng time/s
CW RU	DR- CNN	88.44	85.83	87. 02	12.34
	MSCN N	89.37	90.19	90. 73	14.67
	VMD- SVM	90.21	92.14	93. 03	10.45
	Our model	95.73	94.58	95. 18	8.33
IMS	DR- CNN	87.44	82.37	84. 45	14.21
	MSCN N	89.86	87.56	86. 48	13.58
	VMD- SVM	91.57	91.28	91. 37	11.34
	Our model	95.02	93.22	94. 14	8.07

## 3.2. Simulation testing of the fault diagnosis model for motor rolling bearings

The proposed model is tested in practical applications using the CWRU dataset as an example.

The motor test bench uses a motor power of 1521W and a sampling frequency of 12 kHz. The motor output position uses a pair of torque sensors to collect the output data, and the fault implantation method adopts single point damage of electric discharge machining. Table 2 displays the specific experimental motor parameters.

On the basis of the motor parameters, signal classification tests are conducted on four conditions, as presented in Figure 10.

Figure 10 shows the signal classification test results of DR-CNN, MSCNN, VMD-SVM, and the proposed model for four types of operating states. From Figure 10, there was partial overlap between the signals of normal operation and rolling element faults in the classification results of the DR-CNN method, resulting in significant misclassification. MSCNN has slightly improved classification accuracy, but there are still significant confusion areas between inner and outer ring faults. In addition, the classification performance of VMD-SVM has improved compared to the previous two methods, especially in distinguishing between inner ring faults and rolling element faults. However, the proposed model has the clearest classification boundary. The signal distribution of the four operating states has good clustering effect without obvious overlap, indicating that the IGWS-SVM has higher accuracy and reliability in fault classification tasks. The improved model is more effective in extracting fault features and achieving accurate classification. Finally, the existing fault diagnosis models are compared and tested using Mean Squared Error (MSE), Root Mean Squared Error (RMSE), and Mean Absolute Error (MAE) as reference indicators, as presented in Table 3.

Table 2. Experimental motor parameters

				•	•
Collection location	Speed (r/min)	Fault type	Fault depth (mm)	Fault width (mm)	Sampling frequency (Hz)
Driving end	1500,1550,1600	No fault	No	No	12000
Driving end	1500	Outer ring pitting	0.18	0.05	48000
Driving end	1550	Outer ring spalling	0.36	0.08	48000
Driving end	1600	Outer ring pitting	0.54	0.11	48000
Driving end	1500	Inner ring pitting	0.17	0.04	48000
Driving end	1550	Inner ring spalling	0.36	0.08	48000
Driving end	1600	Inner ring pitting	0.58	0.11	48000
Driving end	1500	Rolling element pitting	0.17	0.04	48000
Driving end	1550	Rolling element spalling	0.35	0.07	48000
Driving end	1600	Rolling element pitting	0.65	0.18	48000

### Chang L. Design of motor bearing fault diagnosis method based on IMPROVED GWO-SVM

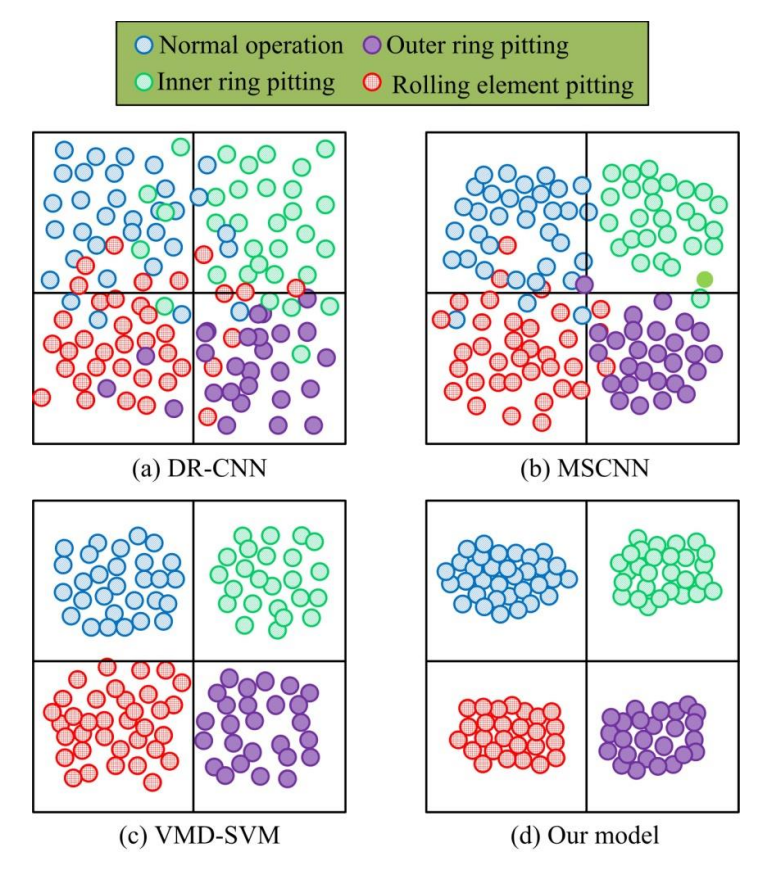


Fig. 10. Signal classification test for different fault types

Table 3. Diagnostic error results

Fault type	Method	MSE	RMSE	MAE	Mean time to diagnosis/s
	DR-CNN	0.134	0.366	0.287	12.45
Outon sing mitting	MSCNN	0.119	0.345	0.268	10.92
Outer ring pitting	VMD-SVM	0.093	0.304	0.237	9.21
	Our model	0.072	0.268	0.189	7.33
	DR-CNN	0.147	0.383	0.299	13.02
Inner ring pitting	MSCNN	0.131	0.362	0.278	11.11
filler fillg pitting	VMD-SVM	0.101	0.318	0.245	9.83
	Our model	0.082	0.286	0.192	7.58
	DR-CNN	0.162	0.402	0.312	14.25
Rolling element spalling	MSCNN	0.148	0.384	0.298	11.89
Koning element spaning	VMD-SVM	0.114	0.337	0.261	10.33
	Our model	0.094	0.306	0.215	8.04

According to Table 3, the proposed model showed the best performance for outer ring faults, with MSE, RMSE, and MAE of 0.072, 0.268, and 0.189, respectively, all significantly better than other comparison models. At the same time, the diagnosis time was the shortest, only 7.33s, far lower than the 12.45s of DR-CNN. This indicates that the improved IGWS-SVM model improves accuracy. In the testing of rolling element spalling faults, the proposed model proposed performed equally well, with RMSE and MAE of 0.306 and 0.215, respectively, which were reduced by about 9.2% and 17.6% compared to VMD-SVM. In addition, the average diagnosis time was 8.04s, which was 6.21s less than the traditional deep learning method DR-CNN, reflecting the advantage of the model in

complex fault feature processing. Overall, the IGWS-SVM model outperforms other methods in various indicators, especially on high accuracy and low consumption, verifying the effectiveness and robustness for rolling BFD tasks.

### 4. CONCLUSION

Aiming at the shortcomings of traditional methods in extracting non-stationary signal features and optimizing hyperparameters for rolling BFD, a signal reconstruction and classification method on the basis of EEMD and SVM was designed, and an improved GWO was introduced for SVM optimization. A new type of electric motor rolling BFD model was proposed. When the three types of

guiding factors of  $\alpha$ ,  $\beta$ , and  $\delta$  were 0.5, 0.4, and 0.7, the loss function value of the model reached a minimum of 0.05, exhibiting better convergence speed and stability. Compared to individual SVM, GWO, or GWO-SVM, the IGWO-SVM proposed in the study achieved a classification accuracy of up to 96.6%, and its performance was significantly improved. At this point, the minimum number of iterations was only 180. Compared with other advanced diagnostic methods, the model had the best precision of 95.73%, the best recall of 94.58%, the best F1 of 95.18%, and the shortest running time of 8.07 seconds. The classification and detection in the CWRU dataset showed that the signal distribution under the proposed model had good clustering effect and no obvious overlap phenomenon was observed. Quantitative data showed that the proposed model had lower detection errors for three types of faults, especially for outer faults. Its MSE, RMSE, and MAE were 0.072, 0.268, and 0.189, respectively, outperforming other comparison models. Due to its modular design, the proposed diagnostic framework has a high degree of scalability. If appropriate signal features are extracted, IGWO optimization and SVM classification can be applied to other fault detection tasks, such as gear defects, rotor unbalance, and even non mechanical anomalies such as power quality disturbances. In summary, the IGWS-SVM rolling bearing fault diagnosis model proposed by the research institute has outstanding performance in accuracy and robustness, and has significant advantages. By introducing dynamic guidance factors and backup position strategies, the global search capability and local convergence efficiency of the GWO algorithm have been effectively improved, avoiding the model from falling into local optima. By combining the structure of EEMD and SVM, efficient extraction and classification of nonstationary vibration signal features have been achieved, enhancing the model's adaptability to complex working conditions. However, this method still has certain limitations, and its diagnostic performance largely depends on the quality of feature decomposition. Improper EEMD parameter settings may affect the stability of the results. In the future, we will further explore end-to-end deep learning architectures to simplify model processes, enhance real-time performance, and deployment flexibility.

**Source of funding:** This research received no external funding.

**Declaration of competing interest**: The author declares no conflict of interest.

#### REFERENCES

 He F, Ye Q. A bearing fault diagnosis method based on wavelet packet transform and convolutional neural network optimized by simulated annealing algorithm.

- Sensors. 2022;22(4):1410-1417. https://doi.org/10.3390/s22041410.
- Liu Y, Kang J, Bai Y, Guo C. A novel adaptive fault diagnosis algorithm for multi-machine equipment: application in bearing and diesel engine. Structural Health Monitoring. 2023;22(3):1677-1707. https://doi.org/10.1177/14759217221113323.
- 3. Dong Y, Wen C, Wang Z. A motor bearing fault diagnosis method based on multi-source data and one-dimensional lightweight convolution neural network. Proceedings of the Institution of Mechanical Engineers, Part I: Journal of Systems and Control Engineering. 2023;237(2):272-283. https://doi.org/10.1177/09596518221124785.
- Zhukovskiy Y, Buldysko A, Revin I. Induction motor bearing fault diagnosis based on singular value decomposition of the stator current. Energies. 2023; 16(8):33033309. <a href="https://doi.org/10.3390/en16083303">https://doi.org/10.3390/en16083303</a>.
- 5. Xu C, Li J, Cheng X. Comprehensive learning particle swarm optimized fuzzy petri net for motor-bearing fault diagnosis. Machines. 2022;10(11):1022-1031. <a href="https://doi.org/10.3390/machines10111022">https://doi.org/10.3390/machines10111022</a>.
- Wang X, Li A, Han G. A deep-learning-based fault diagnosis method of industrial bearings using multisource information. Applied Sciences. 2023;13(2): 933-936. https://doi.org/10.3390/app13020933.
- Song X, Wei W, Zhou J, Ji G, Hussain G, Xiao M, Geng G. Bayesian-optimized hybrid kernel SVM for rolling bearing fault diagnosis. Sensors 2023; 23(11): 5137-5139. https://doi.org/10.3390/s23115137.
- Brusamarello B, Da Silva JCC, de Morais Sousa K, Guarneri GA. Bearing fault detection in three-phase induction motors using support vector machine and fiber Bragg grating. IEEE Sensors Journal. 2022; 23(5):4413-4421. https://doi.org/10.1109/JSEN.2022.3167632.
- 9. Zhou J, Xiao M, Niu Y, Ji G. Rolling bearing fault diagnosis based on WGWOA-VMD-SVM. Sensors. 2022;22(16):6281-6289. https://doi.org/10.3390/s22166281.
- 10. Yang K, Zhao L, Wang C. A new intelligent bearing fault diagnosis model based on triplet network and SVM. Scientific Reports. 2022;12(1):5234-5237. https://doi.org/10.1038/s41598-022-08956-w.
- 11. Wang X, Meng R, Wang G, Liu X, Lu D. The research on fault diagnosis of rolling bearing based on current signal CNN-SVM. Measurement Science and Technology. 2023;34(12):1250-1257. https://doi.org/10.1088/1361-6501/acefed.
- 12. Hakim M, Omran AAB, Ahmed AN, Waily MA, Abdellatif A. A systematic review of rolling bearing fault diagnoses based on deep learning and transfer learning: Taxonomy, overview, application, open challenges, weaknesses and recommendations. Ain Shams Engineering Journal. 2023;14(4):1945-1947. https://doi.org/10.1016/j.asej.2022.101945.
- 13. Ayas S, Ayas MS. A novel bearing fault diagnosis method using deep residual learning network. Multimedia Tools and Applications 2022; 81(16): 22407-22423. https://doi.org/10.1007/s11042-021-11617-1.
- 14. Khan MA, Asad B, Kudelina K, Vaimann T, Kallaste A. The bearing faults detection methods for electrical machines—the state of the art. Energies. 2022;16(1): 296-302. https://doi.org/10.3390/en16010296.
- Tao H, Qiu J, Chen Y, Stojanovic V, Cheng L. Unsupervised cross-domain rolling bearing fault

- diagnosis based on time-frequency information fusion. Journal of the Franklin Institute. 2023;360(2):1454-1477. https://doi.org/10.1016/j.jfranklin.2022.11.004.
- 16. Afia A, Gougam F, Touzout W, Rahmoune C, Ouelmokhtar H, Benazzouz D. Spectral proper orthogonal decomposition and machine learning algorithms for bearing fault diagnosis. Journal of the Brazilian Society of Mechanical Sciences and Engineering. 2023;45(10):550.
  - https://doi.org/10.1007/s40430-023-04451-z.
- 17. Xiong J, Liu M, Li C, Cen J, Zhang Q, Liu Q. A bearing fault diagnosis method based on improved mutual dimensionless and deep learning. IEEE Sensors Journal. 2023;23(16):18338-18348. https://doi.org/10.1109/JSEN.2023.3264870.
- 18. He D, Lao Z, Jin Z, He C, Shan S, Miao J. Train bearing fault diagnosis based on multi-sensor data fusion and dual-scale residual network. Nonlinear Dynamics. 2023;111(16):14901-14924.
  - https://doi.org/10.1007/s11071-023-08638-w.
- Zhang W, Chen D, Xiao Y, Yin H. Semi-supervised contrast learning based on multiscale attention and multitarget contrast learning for bearing fault diagnosis. IEEE Transactions on Industrial Informatics. 2023;19(10):10056-10068.
  - https://doi.org/10.1109/TII.2023.3233960.
- 20. Pal S, Roy A, Shivakumara P, Pal U. Adapting a swin transformer for license plate number and text detection in drone images. Artificial Intelligence and Applications. 2023;1(3):145-154. https://doi.org/10.47852/bonviewAIA3202549.



**Lijuan CHANG** obtained her Bachelor of Engineering (BE) in Mechanical Design, Manufacturing and Automation from Anyang Institute of Technology in 2008. She currently serves as a Lecturer at the School of Intelligent Manufacturing,

Hebi Polytechnic. Her research interests include mechanical design, mechanical manufacturing, and intelligent manufacturing.

e-mail: changlijuan100@163.com